JACS
JOURNAL OF THE AMERICAN CHEMICAL SOCIETY
Communication
pubs.acs.org/JACS

Facile Large-Scale Synthesis of Monodisperse Mesoporous Silica Nanospheres with Tunable Pore Structure

Kun Zhang,*[,†] Lang-Lang Xu,[†] Jin-Gang Jiang,[†] Nathalie Calin,[‡] Koon-Fung Lam,[∥] San-Jun Zhang,[§] Hai-Hong Wu,*[,†] Guang-Dong Wu,[†] Bélen Albela,[‡] Laurent Bonneviot,*[,‡] and Peng Wu[†]

[†]Shanghai Key Laboratory of Green Chemistry and Chemical Processes, Department of Chemistry, East China Normal University, Shanghai, China

[‡]Laboratoire de Chimie, UMR-CNRS 5182, École Normale Supérieure de Lyon, Université de Lyon, Lyon, France

[§]State Key Laboratory of Precision Spectroscopy, East China Normal University, Shanghai, China

[∥]Department of Chemical Engineering, University College London, Torrington Place, London, United Kingdom

Supporting Information

ABSTRACT: Mesoporous silica nanoparticles (MSNs) are experiencing rapid development in the biomedical field for imaging and for use in heterogeneous catalysis. Although the synthesis of MSNs with various morphologies and particle sizes has been reported, synthesis of a pore network with monodispersion control below 200 nm is still challenging. We achieved this goal using mild conditions. The reaction occurred at atmospheric pressure with a templating sol−gel technique using cetyltrimethylammonium (CTA^+) as the templating surfactant and small organic amines (SOAs) as the mineralizing agent. Production of small pore sizes was performed for the first time, using pure and redispersible monodispersed porous nanophases with either stellate (ST) or raspberry-like (RB) channel morphologies. Tosylate (Tos^-) counterions favored ST and bromide (Br^-) RB morphologies at ultralow SOA concentrations. Both anions yielded a worm-like (WO) morphology at high SOA concentrations. A three-step formation mechanism based on self-assembly and ion competition at the electrical palisade of micelles is proposed. Facile recovery and redispersion using specific SOAs allowed a high yield production at the kilogram scale. This novel technique has practical applications in industry.

Considerable progress has been made in the past decade in the synthesis of mesoporous materials with a defined topology and morphology.[1−5] The synthesis of surfactant templated mesoporous silica nanoparticles (MSNs) smaller than 200 nm is emphasized because of their potential applications in cell imaging, disease diagnosis, drug/gene/protein storage or delivery, separation, and heterogeneous catalysis.[6−11] Chemical stability, consistent pore structure, easy large-scale purification, and recovery from colloidal solutions are required for any industrial application of MSNs.[12−17]

Soft-templating synthesis of MSNs is the best and easiest method because there is little aggregation, involving a well-defined pore structure, uniform morphologies, and particle size control. Polymorphic and polydispersed MSNs are produced under kinetic control using dilution and acid quenching.[14,15]

Table 1. Textural Characteristics of Calcined MSNs Synthesized in Various Reaction Conditions

sample[a]	S_{BET}[b] (m^2/g)	V_{total}[c] (mL/g)	V_{inter}[d] (mL/g)	D_{BJH}[e] (nm)	PSD[f] (nm)
MSN-L-T1	435	2.13	0.32	54	74 ± 8
MSN-L-T2	552	1.45	0.41	16	115 ± 10
MSN-L-T3	590	1.38	0.42	17	130 ± 12
MSN-L-B2	675	1.27	0.43	2.3/54	40 ± 3
MSN-H-T2	837	1.71	0.64	2.9/54	90 ± 12
MSN−H-B2[g]	1154	1.58	1.00	2.7	50 to 80

[a]L and H stand for low and high $TEAH_3$/TEOS molar ratio, x = 0.026 and 8.0; T and B stand for Tosylate (Tos^-) and bromide (Br^-) counterions; n stands for SOA with **1** = TEA, **2** = $TEAH_3$, and **3** = AHMPD, respectively. [b]S_{BET} is the specific surface area measured from N2 physisorption. [c]V_{total} is the total internal pore volume measured at P/P_o = 0.99. [d]V_{inter} is the internal pore volume measured at P/P_o = 0.80. [e]D_{BJH} is the pore diameter calculated from the BJH theoretical model (add *ca.* 0.7 nm for BdB or DFT equivalent). [f]Particle size distribution (PSD) was determined by measuring the diameters of at least 100 particles under TEM (Figure S1). [g]From ref 18.

Growth inhibitor additives, such as a triblock copolymer (F127),[12] triethanol amines ($TEAH_3$),[18−20] and functional organosilanes, improve the process, resulting in better particle size control. Without the addition of any additives, control of pore size and structure is poor.[13,21,22] Several groups have synthesized MSNs with radial-oriented mesochannels and a conical pore shape using microemulsion media.[23−26] These stellate structures are ideal scaffolds for biological, medical, and catalytic applications, as the pore structures are accessible by large molecules.[27−29] These structures are either too large (>200 nm) for application in life sciences or too complex to be produced at a large scale. Thus, reliable large-scale production of MSNs with tunable porosity and particle size, particularly <200 nm, is highly desirable.[12−26,30]

In this work, the first kilogram scale synthesis of pure nanophases of monodisperse MSNs smaller than 130 nm with stellate (ST), raspberry (RB), or worm-like (WO) morphol-

Received: November 29, 2012
Published: January 30, 2013

dx.doi.org/10.1021/ja3116873 | J. Am. Chem. Soc. 2013, 135, 2427−2430

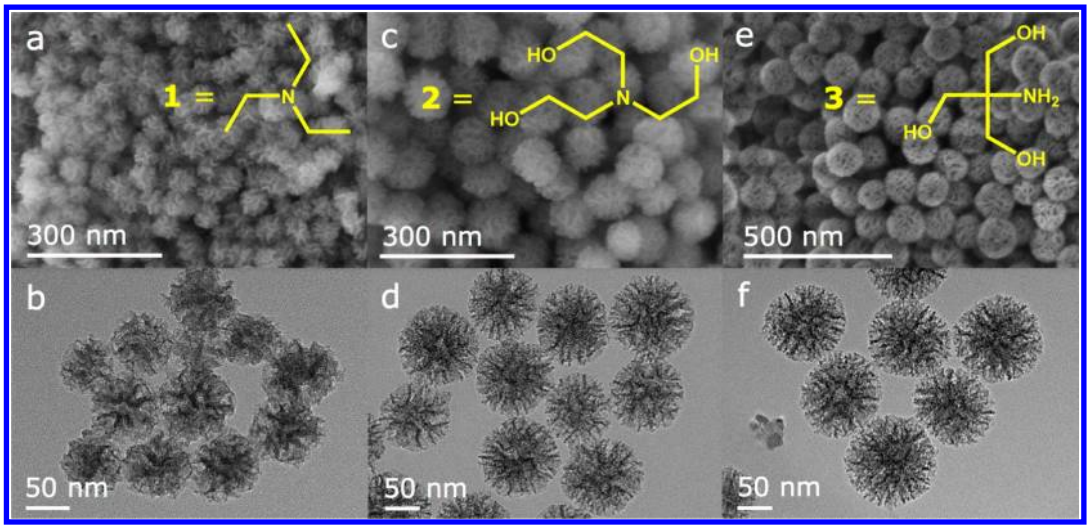

Figure 1. SEM (top) and TEM (bottom) images of MSN-L-T1 (a, b), MSN-L-T2 (c, d), MSN-L-T3 (e, f).

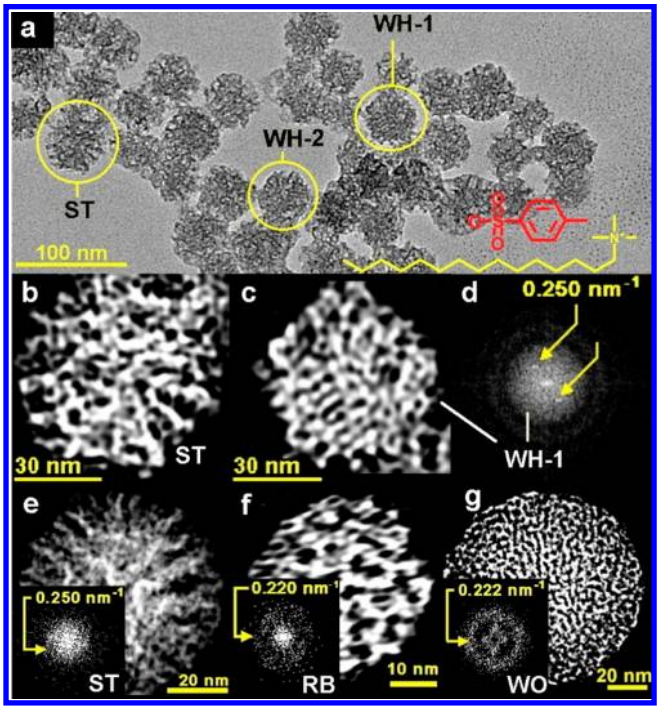

Figure 2. HRTEM images of MSNs synthesized (a) at an intermediate concentration of **2**, x = 2.0 (average size 60 ± 6 nm) with inverted contrast (bottom right: surfactant formula with Tos^- counterion), (b) the ST MSN indicated in "a", (c) WH-1, (d) diffraction pattern of WH-1, (e) ST MSN from MSN-L-T-2, (f) RB MSN from MSN-B-2 (Figure 3), and (g) WO MSNs from MSN-H-T2 (see TEM in Figure S6a) (insert: diffraction pattern).

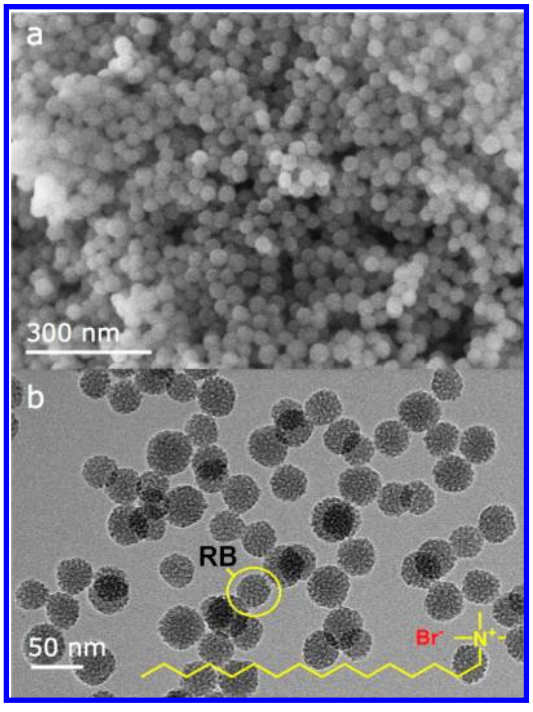

Figure 3. SEM (a) and HR-TEM (b) images of MSN-L-B2. The highlighted RB MSN was shown in inverted contrast in Figure 2f (bottom: formula of the surfactant with Br^- as counterion).

ogies was developed based on the nature and the concentration of small organic amines (SOA) together with an appropriate choice of the cationic surfactant counterions. The MSNs were easily separated and collected by filtration when the SOAs such as triethanolamine, $TEAH_3$ = **2** and 2-amino-2-(hydroxymethyl)propane-1,3-diol, AHMPD = **3** were used instead of triethyleneamine, TEA = **1**. Indeed, 2 and 3 were the only to possess multiple hydrogen bonding capacities. A formation mechanism was proposed for fine-tuning of the channel morphologies.

The synthesis was performed under room conditions with a typical mother liquor composition of $1.0SiO_2$:0.06CTATos:xSOA:$80H_2O$ at a molar basis, where x (SOA/TEOS) varied from 0.026 to 8.0. In a typical large-scale synthesis of stellate MSNs, 1458.0 g of tetraethylorthosilicate (TEOS), 192.0 g of cetyltrimethyl-ammonium (CTA^+) tosylate, and 34.7 g of **2** or 22.1 g of **3** were dissolved in 10 L of water. The reaction was carried out at 80 °C for 2 h. The final pH was *ca.* 7 and 10 at x = 0.026 and 8.0, respectively. After filtration and drying at 100 °C for 20 h, 460 to 600 g were collected (93% and 85% yield for SiO_2 and the surfactant), respectively for MSN-L-T2 and MSN-L-T3 (the sample nomenclature and more details on synthesis available in the Supporting Information, SI).

dx.doi.org/10.1021/ja3116873 | *J. Am. Chem. Soc.* 2013, 135, 2427−2430

Scheme 1. Synthesis Mechanisms at Low or High SOA (green dots) Concentration (pH ≈ 7 or 10) and Tos^- (left) or Br^- (middle) (template counterion is not represented here)[a]

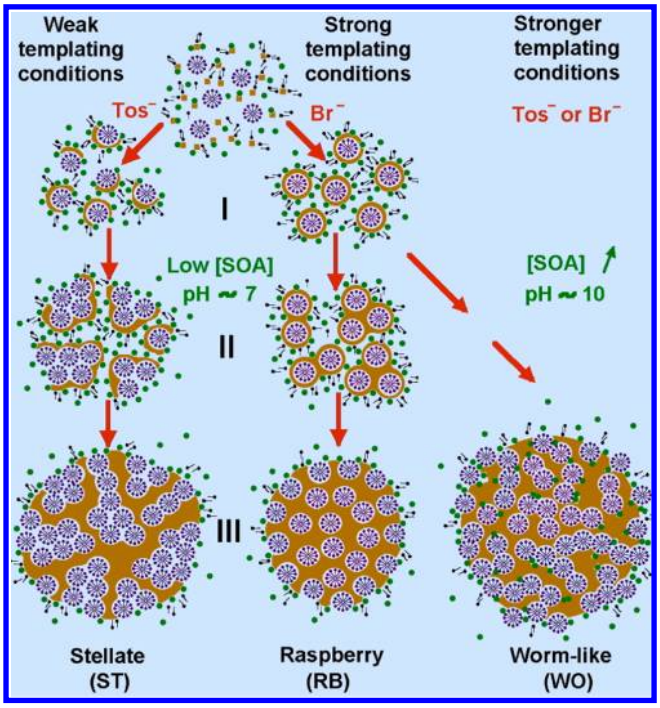

[a](I) partly silicated micelles, (II) block formation, and (III) block aggregation into stellate or raspberry nanoparticles.

When CTATos were used as the template, particles were spherical with an ST morphology. Average sizes increased from 74 to 130 nm as **1** to **3** were used (Figures 1 and S1, Table 1). For **2** and **3**, TEM determined the average pore mouth diameter to be *ca.* 10 and 15 nm, using N_2 physisorption (Figure S2). For **1**, the pore mouths were slightly larger, ~20 nm, and not resolved due to the interparticle voids from the N_2 adsorption isotherm. Larger surface areas and internal pore volumes were consistent not only with full pore connectivity but also with thinner and more tortuous walls for **2** and **3** (Figure 1b, d, f).

High-rate centrifugation is necessary to recover MSN-L-T1 for small nanoparticles.[12−26,30] However, when **2** and **3** were used instead of **1**, filtration was sufficient for the separation. Moreover, after ultrasonic treatment, the MSNs were totally redispersed in either water or ethanol, but not in cyclohexane or toluene (Figure S3). The MSNs were apparently held together in aggregates which were large enough to be separated by filtration alone. The formation of similar metastable nanoflocculates was also observed with zeolite nanoparticles.[31] The amine molecules **2** and **3** were protonated at pH 7−10 and were likely to interact with silicate more strongly than **1** because of the chelating properties of the ethanol arms (pK_a in SI). Moreover, molecules **2** and **3**, with four H-bonding centers, favored the formation of dense networks of bridging particles. Both effects may explain the flocculate dismantlement and particle redispersion seen in polar-protic solvents.

The channel morphology was first adjusted by varying x. At x = 0.026, all particles were ST typed and did not present any diffraction pattern (Figures 1, 2e, and S4). At the intermediate values ($x \geq 2.0$), a broad XRD peak appeared at $2\theta = 1.7°$ and a new type of particle with worm-like and parallel pore channels was seen (Figure 2a). These MSNs exhibited two diffraction dots with a reciprocal distance of 0.250 nm^{-1} assigned to the parallel channels, prefiguring a nascent hexagonal phase (Figures 2c and 2d). These transitional particles, denoted as WH (Worm−Hexagonal transition state), possessed flat edges (parallel channels, Figure 2d). This transition was bypassed as the WO morphology was solely attained at high x value (Figures S5a and S6a). A similar WO nanophase was reported using Br^- instead of Tos^- counterions and also with a high x value (reported in Table 1 as MSN-H-B2).[18] Such morphology was characterized by a single X-ray diffraction peak and a single electron diffraction ring (Figures S4 and 2g).[14,15,18] The ST-WH-WO nanophase transition was accompanied by an evolution from regular spheres to ill-faceted and again to spherical particles with larger porosities (up to 1.71 mL/g) and higher surface areas (up to 837 m^2/g). It is worth noting that the formation of geminates and rows of sealed nanoparticles at high SOA/TEOS molar ratios (>1) was consistent with an increased viscosity that favored slow kinetics and fusion of particles (Figures S5 and S6).

At the molecular level, the curvature of the organic−inorganic electrical interface was affected by the counterions (X^-) remaining in the material. This can be described as $\{(1 + n)S^+, nX^-, I^-\}$ with S^+ standing for CTA^+ and I^- for the negatively charged silica surface.[32,33] The presence of Tos^- in the stellate MSNs was confirmed by ^{13}C CP MAS NMR and thermogravimetric analysis (Figures S7−S9). Under similar synthesis conditions, the substitution of Br^- ions led to monodispersed quasi-spherical MSNs with spherical pores. Such a raspberry-like morphology was previously described only in polymorphic and polydispersed systems obtained by using both dilution and pH quenching (Figures 2f and 3).[15] The structural uniformity of the MSNs allowed the first consistent measurement of pore size (*ca.* 2.3 nm) from both TEM and N_2 physisorption isotherms and confirmed the pore templating mechanism by single spherical CTA^+ micelles, as proposed earlier.[15] Connection to the exterior was confirmed by the large surface area and pore volume (Figures 2f and 3b, Table 1). The pivotal role of the counterions in forming the pore network is rationalized by the much lower affinity of Br^- than Tos^- for the electrical palisade of the CTA^+ micelles (lower CMC for CTATos than CTABr).[34−36] Tos^- competes more against the adsorption of silicate oligomers on the micelles than Br^-. This competition is favored at low pH (obtained at low SOA concentrations). As a consequence, the concentration of Tos^- is high in the MSNs (Figures S7−S9). Indeed, the silanolate density (I^-) is too small to displace Tos^- anions efficiently. We named this phenomenon "weak templating" conditions.[37] In contrast, high SOA concentrations (pH ≈ 10) and high silanolate density result in stronger templating conditions, yielding Tos^--poor MSNs with a more organized 1D worm-like array of the pore channels. The highly ordered 2D hexagonal LUS silica poorly adsorbs Tos^-, despite the similarity in gel composition and pH.[32,33,38] The difference may be due to the presence of SOAs. The rationale may come from a cationic competition between SOAs still protonated at pH 10 and CTA^+, thus deteriorating the templating at high x ratios.

The high thermal stability of the actual MSNs (better than that of SBA-15 mesophases) in saturated steam at 700 °C occurred because of the denser and thicker pore walls. These are in agreement with the TEM observations and low silanol

dx.doi.org/10.1021/ja3116873 | J. Am. Chem. Soc. 2013, 135, 2427−2430

concentrations seen using NMR (Q_3 measured using ^{29}Si MAS NMR spectra, Figures S10−S13).[39] The stability was related to the catalytic properties of amine **1** and the aminoalcohols **2** and **3** that allowed silicate condensation at neutral pH, similar to other polyamines or polyols moieties in protein producing biogenic silicas.[40−42]

Although the formation of stellate channel morphology may suggest kinetically driven growth by percolation on aggregated micelles, a self-assembly of partially silicated micelles as depicted in Scheme 1 is more likely to occur with respect to the surfactant concentration that is below the surfactant CMC.[1−5,32,39] We believe that the three-step formation mechanism is appropriate for describing the synthesis of all three types of MSN morphologies, in which self-assembly takes place between polymerizing silicate oligomers and individual surfactant micelles. The imperfect-centered stellate shape morphology suggests that the growth proceeds via a block-by-block aggregation, similar to that seen in zeolite.[31] The mesochannel morphology is controlled by the template counterion and the SOA concentration, yielding tighter templating conditions and silicated micelles. Stellate nanophases smaller than 130 nm and pure raspberry-like channel nanophases were obtained for the first time with this technique. SOAs acted as soft particle binders, allowing easy recovery, redispersion, and a high yield large-scale production of MSNs.

■ ASSOCIATED CONTENT

Supporting Information

Experimental details, characterization data, and supporting figures. This material is available free of charge via the Internet at http://pubs.acs.org.

■ AUTHOR INFORMATION

Corresponding Author

kzhang@chem.ecnu.edu.cn; hhwu@chem.ecnu.edu.cn; Laurent.bonneviot@ens-lyon.fr

Notes

The authors declare no competing financial interest.

■ ACKNOWLEDGMENTS

This work was supported by the NSFC (21003050, 20925310, U1162102, 61008003), the STCSM (10ZR1410500, 08DZ2273300, 11QA1402100), the Ph.D. Programs Foundation of the Ministry of Education of China (20100076120019), the National Key Technology R&D Program (2012BAE05B02), the innovation Program of Shanghai Municipal Education Commission (13ZZ038), the Fundamental Research Funds for the Central Universities and the Joint Research Institute for Science and Society (JoRISS) of ECNU, ENS de Lyon, and CNRS.

■ REFERENCES

(1) Wan, Y.; Zhao, D. Y. *Chem. Rev.* **2007**, *107*, 2821−2860.
(2) Wan, Y.; Yang, H. F.; Zhao, D. Y. *Acc. Chem. Res.* **2006**, *39*, 423−432.
(3) Gao, C. B.; Che, S. A. *Adv. Funct. Mater.* **2010**, *20*, 2750−2768.
(4) Taguchi, A.; Schüth, F. *Microporous Mesoporous Mater.* **2005**, *77*, 1−45.
(5) Martín-Aranda, R. M.; Čejka, J. *Top. Catal.* **2010**, *53*, 141−153.
(6) Xie, J.; Lee, S.; Chen, X. *Adv. Drug Delivery Rev.* **2010**, *62*, 1064−1079.
(7) Rosenholm, J. M.; Sahlgren, C.; Lindén, M. *Nanoscale* **2010**, *2*, 1870−1883.
(8) Vivero-Escoto, J. L.; Slowing, I. I.; Trewyn, B. G.; Lin, V. S.-Y. *Small* **2010**, *6*, 1952−1967.
(9) He, Q.; Shi, J. *J. Mater. Chem.* **2011**, *21*, 5845−5855.
(10) Wu, S. H.; Hung, Y.; Mou, C. Y. *Chem. Commun.* **2011**, *47*, 9972−9985.
(11) Du, X.; He, J. H. *Nanoscale* **2011**, *3*, 3984−4002.
(12) Suzuki, K.; Ikari, K.; Imai, H. *J. Am. Chem. Soc.* **2004**, *126*, 462−463.
(13) Paula, A. J.; Montoro, L. A.; Fiiho, A. G.; Alves, O. L. *Chem. Commun.* **2012**, *48*, 591−593.
(14) Fowler, C. E.; Khushalani, D.; Lebeau, B.; Mann, S. *Adv. Mater.* **2001**, *13*, 649−652.
(15) Sadasivan, S.; Fowler, C. E.; Khushalani, D.; Mann, S. *Angew. Chem., Int. Ed.* **2002**, *41*, 2151−2153.
(16) Lin, Y. S.; Abadeer, N.; Hurly, K. R.; Haynes, C. L. *J. Am. Chem. Soc.* **2011**, *133*, 20444−20457.
(17) Hollamby, M. J.; Borisova, D.; Brown, P.; Eastoe, J.; Grillo, I.; Shchukin, D. *Langmuir* **2012**, *28*, 4425−4433.
(18) Möller, K.; Kobler, J.; Bein, T. *Adv. Funct. Mater.* **2007**, *17*, 605−612.
(19) Urata, C.; Aoyama, Y.; Tonegawa, A.; Yamauchi, Y.; Kuroda, K. *Chem. Commun.* **2009**, *45*, 5094−5096.
(20) Zhang, K.; Zhang, Y.; Hou, Q. W.; Yuan, E. H.; Jiang, J. G.; Albela, B.; He, M. Y.; Bonneviot, L. *Microporous Mesoporous Mater.* **2011**, *143*, 401−405.
(21) Cauda, V.; Schlossbauer, A.; Kecht, J.; Zürner, A.; Bein, T. *J. Am. Chem. Soc.* **2009**, *131*, 11361−11370.
(22) Huh, S.; Wiench, J. W.; Trewyn, B. G.; Song, S.; Pruski, M.; Lin, V. S.-Y. *Chem. Commun.* **2003**, *39*, 2364−2365.
(23) Polshettiwar, V.; Cha, D.; Zhang, X. X.; Basset, J. M. *Angew. Chem. Int. Ed.* **2010**, *49*, 9652−9656.
(24) Zhang, H. J.; Li, Z. Y.; Xu, P. P.; Wu, R. F.; Jiao, Z. *Chem. Commun.* **2010**, *46*, 6783−6785.
(25) Du, X.; He, J. H. *Langmuir* **2010**, *26*, 10057−10062.
(26) Nandiyanto, A. B. D.; Kim, S. G.; Iskandar, F.; Okuyama, K. *Microporous Mesoporous Mater.* **2009**, *120*, 447−453.
(27) Deng, Y. H.; Cai, Y.; Sun, Z. K.; Zhao, D. Y. *Chem. Phys. Lett.* **2011**, *510*, 11−13.
(28) Deng, Y. H.; Cai, Y.; Sun, Z. K.; Liu, J.; Liu, C.; Wei, J.; Li, W.; Liu, C.; Wang, Y.; Zhao, D. Y. *J. Am. Chem. Soc.* **2010**, *132*, 8466−8473.
(29) Deng, Y. H.; Qi, D. W.; Deng, C. H.; Zhang, X. M.; Zhao, D. Y. *J. Am. Chem. Soc.* **2008**, *130*, 28−29.
(30) Qiao, Z. A.; Zhang, L.; Guo, M. Y.; Liu, Y. L.; Huo, Q. S. *Chem. Mater.* **2009**, *21*, 3823−3829.
(31) Gao, F.; Sougrat, R.; Albela, B.; Bonneviot, L. *J. Phys. Chem. C* **2011**, *115*, 7285−7291.
(32) Badiei, A.-R.; Cantournet, S.; Morin, M.; Bonneviot, L. *Langmuir* **1998**, *14*, 7087−7090.
(33) Echchahed, B.; Morin, M.; Blais, S.; Badiei, A. R.; Berhault, G.; Bonneviot, L. *Microporous Mesoporous Mater.* **2001**, *44−45*, 53−63.
(34) Bartet, D.; Gamboa, C.; Sepúlveda, L. *J. Phys. Chem.* **1980**, *84*, 272−275.
(35) Gamboa, C.; Ríos, H.; Sepúlveda, L. *J. Phys. Chem.* **1989**, *93*, 5540−5543.
(36) Bijma, K.; Engberts, J. *Langmuir* **1997**, *13*, 4843−4849.
(37) Muto, S.; Imai, H. *Microporous Mesoporous Mater.* **2006**, *95*, 200−205.
(38) Zhang, K.; Chen, H. L.; Albela, B.; Jiang, J. G.; Wang, Y. M.; He, M. Y.; Bonneviot, L. *Eur. J. Inorg. Chem.* **2011**, 59−67.
(39) Zhao, D. Y.; Feng, J. L.; Huo, Q. S.; Melosh, N.; Fredrickson, G. H; Chmelka, B. F.; Stucky, G. D. *Science* **1998**, *279*, 548−552.
(40) Cha, J.; Shimizu, K.; Zhou, Y.; Christiansen, S. C.; Chmelka, B. F.; Stucky, G. D.; Morse, D. E. *Proc. Natl. Acad. Sci. U.S.A.* **1999**, *96*, 361−365.
(41) Kröger, N.; Deutzmann, R.; Sumper, M. *Science* **1999**, *286*, 1129−1132.
(42) Hartmann, S.; Brandhuber, D. *Acc. Chem. Res.* **2007**, *40*, 885−894.